Numerical Methods for Electromagnetic Modeling of Graphene: A Review

Kaikun Niu, *Member, IEEE*, Ping Li, *Senior Member, IEEE*, Zhixiang Huang, *Senior Member, IEEE*, Li Jun Jiang, *Fellow, IEEE*, and Hakan Bagci, *Senior Member, IEEE*

***Abstract*—Graphene's remarkable electrical, mechanical, thermal, and chemical properties have made this the frontier of many other 2-D materials a focus of significant research interest in the last decade. Many theoretical studies of the physical mechanisms behind these properties have been followed by those investing the graphene's practical use in various fields of engineering. Electromagnetics, optics, and photonics are among these fields, where potential benefits of graphene in improving the device/system performance have been studied. These studies are often carried out using simulation tools. To this end, many numerical methods have been developed to characterize electromagnetic field/wave interactions on graphene sheets and graphene-based devices. In this article, most popular of these methods are reviewed and their advantages and disadvantages are discussed. Numerical examples are provided to demonstrate their applicability to real-life electromagnetic devices and systems.**

***Index Terms*—Computational electromagnetics (CEM), graphene, 2-D materials.**

I. Introduction

GRAPHENE [1], [2], an allotrope of the 3-D crystalline graphite, consists of carbon atoms arranged as a 2-D monolayer of hexagonal lattice resembling a honeycomb. In the last decade, it has attracted significant attention from various research communities in the fields of physics and engineering due to its unprecedented mechanical and electrical properties that have lead to the design of many new systems and devices [3]–[6].

The graphene stacks can be produced on a piece of paper when we write with a pencil since the pencil lead contains graphite consisting of multilayer graphene. Recent technological developments in optical microscopy have permitted the experimental study of atomically thin 2-D materials including graphene. Indeed, Novoselov and Geim [1], who studied the graphene and observed its properties at the beginning of the 21th century, received the Nobel Prize for their groundbreaking contribution. They have found that graphene supports a strong ambipolar electric field effect and demonstrates semimetallic properties. It has also been demonstrated that graphene exhibits electrical characteristics similar to those of the semiconductors (except the zero band gap) [7]. The invention of micromechanical cleavage technique has certified that the high-quality graphene can be isolated easily. This has immediately ignited an evolution in the investigation of a whole family of 2-D materials [8], [9] (whose first member is graphene). The family of 2-D materials has expanded rapidly to include more members and now consists of a large number of materials such as hexagonal boron nitride (insulator) [10], black phosphorus (semiconductor) [11], and $NbSe_2$ (metal) [12]. These 2-D materials can often be stacked together to create novel materials with synergetic effects [13] that can execute a user-desire function.

Significant research has been done to uncover the underlying physics behind the exceptional characteristics of 2-D materials, which are distinctively different from those of their traditional 3-D parental materials. First of all, since 2-D materials are constructed starting from an atomic level, they are weakly restricted by van der Waals forces that hold the material layers together [9]. Second, 2-D materials strongly interact with electromagnetic fields in a broad range of frequencies changing from microwave to ultraviolet part of the spectrum [14], [15]. Third, the quantum Hall and Berry phase effects are observed along the direction of the 2-D material's surface [16]. These novel effects occur on monolayer 2-D materials distinguishing them from their 3-D counterparts and translate to unprecedented optical, electrical, mechanical, and thermal features [17]. These features have opened the way to designing tunable optical and electronic devices with high confinement and low loss and abilities to execute high-speed and flexible light detection, modulation, and manipulation.

Manuscript received January 2, 2020; revised February 27, 2020; accepted March 18, 2020. Date of publication March 30, 2020; date of current version April 30, 2020. This work was supported in part by the National Natural Science Foundation of China under Grant 61701424, Grant 61674105, Grant 61831016, Grant 61971001, Grant 61601166, Grant 61701001, Grant 61701003, and Grant 61701423, in part by the National Natural Science Fund for Excellent Young Scholars under Grant 61722101, and in part by the China Scholarship Council. *(Corresponding author: Ping Li.)*

Kaikun Niu was with the Key Laboratory of Electromagnetic Environmental Sensing, Department of Education of Anhui Province and the Institute of Physical Science and Information Technology, Anhui University, Hefei 230601, China, and is now with the Division of Computer, Electrical, and Mathematical Science and Engineering, King Abdullah University of Science and Technology, Thuwal 23955-6900, Saudi Arabia (e-mail: kaikun.niu@kaust.edu.sa).

Ping Li is with the Key Laboratory of Ministry of Education of China for Research of Design and Electromagnetic Compatibility of High Speed Electronic Systems, Shanghai Jiao Tong University, Shanghai 200240, China, and also with the HKU-SIRI, Shenzhen 518057, China (e-mail: ping.li@sjtu.edu.cn).

Zhixiang Huang is with the Key Laboratory of Electromagnetic Environmental Sensing, Department of Education of Anhui Province and the Institute of Physical Science and Information Technology, Anhui University, Hefei 230601, China (e-mail: zxhuang@ahu.edu.cn).

Li Jun Jiang is with the Department of Electrical and Electronic Engineering, The University of Hong Kong, Hong Kong (e-mail: jianglj@hku.hk).

Hakan Bagci is with the Division of Computer, Electrical, and Mathematical Science and Engineering, King Abdullah University of Science and Technology, Thuwal 23955-6900, Saudi Arabia (e-mail: hakan.bagci@kaust.edu.sa).

Digital Object Identifier 10.1109/JMMCT.2020.2983336

Indeed, in the last several years, many researchers have focused on realizing the potential of graphene in real-life applications. As mentioned above, graphene strongly interacts with electromagnetic fields: Its response to high-frequency electromagnetic field, i.e., light, is nonlinear and shows plasmonic characteristics. This response can be adjusted through doping, gating, and chemical processes [18]. A tunable terahertz (THz) graphene-based metamaterial has been engineered to achieve conspicuous optical absorption peaks through the generation of plasmon resonances [19]. The gigahertz (GHz) graphene-based electro-absorption modulator capable of operating at a wide range of frequencies has been designed by tailoring graphene's Fermi level [20].

The most successful and commonly used device, which makes use of graphene's electronic properties, is the field-effect transistor (FET). Graphene supports an impressively high carrier mobility at room temperature, which in return helps to increase the FET's operation speed [21]. On the other hand, the channel of the logical devices making use of graphene cannot be switched off since graphene has no band gap. To overcome this problem by opening up the band gap, graphene nanoribbon (GNR) [22], and biased bilayer graphene [23] have been proposed and implemented. Furthermore, the possibility of molecular-scale electronics has been certified by the invention of graphene-based quantum dot devices developed to achieve electron transport [24]. It has been demonstrated that a transistor, which is implemented using graphene and boron nitride, supports a negative differential conductance that can be tuned by changing the gate voltage [13]. The first top-gated metal-oxide-semiconductor FET (MOSFET) with graphene has been manufactured to increase carrier mobilities [25]. Graphene has played a prominent role in the design of organic light-emitting diodes (OLEDs) [26], solar cells [27], antennas [28], [29], and frequency multipliers [30].

In addition to experimental investigation of graphene and graphene-based devices, their numerical modeling and simulation have been an important research topic. The Kubo formula provides an analytic expression for the graphene's conductivity and shows that it is a function of several physical parameters including wavelength, temperature, and chemical potential [31], [32]. Moreover, a surface conductivity model, which describes graphene as an infinitesimally thin (two sided) sheet with a local and isotropic conductivity, has been proposed. This model permits derivation of analytical expressions for the electromagnetic field in the presence of a graphene sheet in terms of a dyadic Green function (represented using Sommerfeld integrals) and exciting electric current [33], [34]. Even though these analytical models and methods can provide results for several canonical problems for benchmarking purposes, many practical problems involving graphene, such as design of arbitrarily shaped electromagnetic devices, are analytically intractable. With the recent advances in the field of computational electromagnetics (CEM), various accurate and efficient numerical methods have become available for analysis of electromagnetic field/wave interactions on graphene sheets and/or graphene-based devices [35]. These simulations tools are indispensable components of the design frameworks; they provide constructive guidance that significantly accelerates the design and fabrication process, which would rely on experimental trial and error otherwise. Review papers on experimental investigation of graphene's properties, graphene-based devices, and their applications are widely available [36]–[39]. However, a comprehensive summary of computational tools developed for analyzing graphene-based devices/systems is not found in the literature. The purpose of this review paper is to fill this gap.

In this review article, we focus on recent numerical methods that are formulated and implemented for analysis of electromagnetic field/wave interactions on graphene sheets and graphene-based devices. We discuss advantages and disadvantages of these methods and provide several numerical examples from several influential works to demonstrate their applicability in real-life engineering applications.

II. Simulation Methods for Graphene

In the last few decades, increasing CPU speed and availability of memory on computers as well as the development of new efficient and accurate algorithms have rendered electromagnetic simulation tools more applicable than ever. To analyze electromagnetic field/wave interactions on graphene sheets and graphene-based devices, one can use several different frequency domain (FD) and time domain (TD) numerical methods including finite-difference time-domain (FDTD) method, discontinuous Galerkin time-domain (DGTD) method, finite element method (FEM), and method of moments (MoM). These methods discretize and solve Maxwell or Helmholtz equations or their integral equation (IE) representations. Regardless of the domain they operate in (frequency or time), these methods call for a mathematical model for graphene's conductivity. This mathematical model is described in the following section, which is followed by the review of the numerical methods mentioned above.

A. Mathematical Model

Numerical methods listed previously often model graphene as a thin surface with complex and frequency-dependent/dispersive conductivity. This frequency-dependence suggests that a FD analysis is more adequate since a TD method requires the additional step of converting frequency dependence into the TD. The surface conductivity of graphene is often expressed using the Kubo formula [31], [33], [40]

$$\sigma_d = \frac{je^2\left(\omega - j2\Gamma\right)}{\pi\hbar^2}\left[-\int_0^\infty \varepsilon \frac{f_d\left(-\varepsilon\right) - f_d\left(\varepsilon\right)}{\left(\omega - j2\Gamma\right)^2 - 4\left(\varepsilon/\hbar\right)^2} d\varepsilon + \frac{1}{\left(\omega - j2\Gamma\right)^2}\int_0^\infty \varepsilon\left(\frac{\partial f_d\left(\varepsilon\right)}{\partial\varepsilon} - \frac{\partial f_d\left(-\varepsilon\right)}{\partial\varepsilon}\right) d\varepsilon\right] \quad (1)$$

where ω is the radian frequency, Γ is the phenomenological electron scattering rate (in some literature, the phenomenological electron relaxation rate/time $\tau = 1/(2\Gamma)$ is used to substitute Γ), e is the electron charge, ε is the energy state, and $\hbar$ is the reduced Plank constant. $f_d = (e^{(\varepsilon - |\mu_c|)/k_B T} + 1)^{-1}$ is the

Fermi–Dirac distribution, where T is the temperature, k_B is the Boltzmann constant, and μ_c is the chemical potential (also called Fermi energy) that can be adjusted by the electrostatic bias field, chemical doping, or carrier density. The first and second terms in (1) are due to intraband and interband contributions, respectively. The expression of the intraband contribution reads

$$\sigma_{d,\text{intra}} = -\frac{je^2 k_B T}{\pi\hbar^2\left(\omega - j2\Gamma\right)}\left(\frac{\mu_c}{k_B T} + 2\ln\left(e^{-\frac{\mu_c}{k_B T}} + 1\right)\right). \quad (2)$$

The expression of the interband contribution reads

$$\sigma_{d,\text{inter}} \simeq \frac{-je^2}{4\pi\hbar}\ln\left(\frac{2\left|\mu_c\right| - \left(\omega - j2\Gamma\right)\hbar}{2\left|\mu_c\right| + \left(\omega - j2\Gamma\right)\hbar}\right). \quad (3)$$

The interband conductivity is on the order of $e^2/\hbar$ and smaller than the intraband conductivity. At lower frequencies (i.e., THz region), electrons and holes near the band edges "block" the interband transitions. Graphene behaves like a conductive film and its conductivity (dominated by intraband contribution) can be described in the form of a simple Drude model.

For higher frequencies (i.e., infrared and visible region where μ_c is much smaller than optical frequency $\hbar\nu$), the graphene conductivity is barely dependent on μ_c and $\hbar\nu$ [41]. At these frequencies, the electrons can gather enough excitation energy to jump from an inner band to an upper band and the graphene's conductivity is dominated by interband contribution.

In addition, the formulas given in (1)–(3) are valid under the assumption that the collision rate of carriers (τ^{-1}) is less than the frequency (ω) and spatial dispersion of the EM fields ($k\nu$), i.e., $\omega \gg k\nu, \tau^{-1}$ [42]. It should also be noted here that conductivities of other forms of graphene, such bilayer and multilayer cases are different than that of the monolayer graphene. The conductivity of monolayer and bilayer graphene has been discussed in [43]. The Hamiltonian decomposition, Landau-level structure, and conductivity of multilayer graphene have been investigated in [44]. Additionally, in [45]–[47], the optical and Hall conductivities of monolayer graphene have been studied.

It is clear from the abovementioned equations that graphene's conductivity is a function of chemical potential, temperature, and frequency. This consequently means that the polarization, propagation, and scattering characteristics of the electromagnetic waves interacting with the graphene can be tailored by adjusting these parameters.

TD methods often model the dispersive conductivity of graphene [as shown in (1)–(3)] using an auxiliary difference equation (ADE) in an (unknown) equivalent polarization current. This equation is then solved together with Maxwell equations. The intraband conductivity, whose expression in FD "looks" like a Drude model, is easily converted to TD and expressed in terms of an ADE. However, the interband conductivity has a complex logarithmic form and, therefore, transforming it into TD calls for more general approaches. The first one of these makes use of the Padé approximant spectral fitting model, which is accurate only in the near infrared part of the spectrum [48]. The second approach is termed "vector fitting," where a summation of rational functions (in Laplace domain) of complex conjugate pole-residues pairs, are used to approximate the interband conductivity in a broadband of frequencies. The resulting expression then is converted into TD using the analytical inverse Laplace transform of the rational functions [49], [50].

B. Finite-Difference Time-Domain Method

The FDTD method, first invented by Yee [51] in 1966, is a robust TD method that discretizes the time-dependent Maxwell curl equations by approximating time and space derivatives using finite difference approximations. The unknown time-space samples of the fields/fluxes obtained by solving or through explicit updates of the resulting equations in a recursive manner in time. FDTD is straightforward to implement, suitable for parallel computation, provides results that are immediately ready for visualization, and being a TD method, produces wideband information in a single execution. These advantages have rendered FDTD the first method of choice in many electromagnetic problems in a wideband of frequency ranging from RF to optical frequencies, which require numerical characterization of transient, dispersive, and nonlinear field interactions [52], [53]. Consequently, it should not come as a surprise that FDTD has also become increasingly prevalent in the simulation of graphene-based devices.

There are the following three main approaches to modeling graphene in FDTD-based electromagnetic simulations.

1) A fine grid is used to discretize the graphene while taking into account its finite thickness. For this approach, the surface conductivity is transformed to an equivalent (complex) permittivity [54].
2) A subcell FDTD is used to simulate the thin layers of graphene [55].
3) An impedance boundary condition (IBC) that locally represents the field behavior on a graphene sheet with zero thickness is incorporated into FDTD [56], [57].

For the first approach, the 2-D graphene surface is usually modeled as a 3-D material but with a very thin layer with thickness h. The conductivity of this layer is expressed as

$$\sigma_{3\text{D}} = \frac{\sigma_d}{h}. \quad (4)$$

Then, a traditional FDTD method can make use of an ADE technique to incorporate the Drude model for the graphene's intraband conductivity while ignoring its interband counterpart. To incorporate the interband effects into the simulation, the complex conjugate dispersion material model [58] can be used. In addition, the conformal [59] and high-order modeling techniques [60] have been used together with the FDTD method to improve the accuracy of the simulation. Furthermore, an extended Lorentz model, which is represented in the form of an equivalent circuit [61], has been proposed to take magnetized graphene into account in FDTD simulations.

The thickness of a graphene layer is approximately 0.34 nm and the accuracy of the 3-D conductivity [as described in (4)] reduces with increasing thickness. The nanoscale volumetric mesh resulting from the discretization of the graphene layer leads to a very small time step because of the Courant–Friedrich–Levy

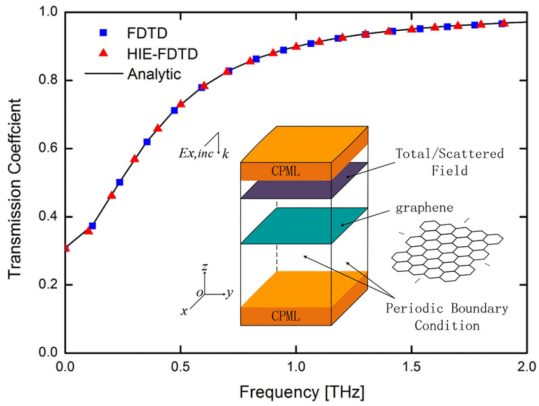

Fig. 1. Transmission coefficient for a plane wave normally incident on an infinite graphene sheet as computed using HIE-FDTD, traditional FDTD, and an analytical expression. Reproduced with permission from [70].

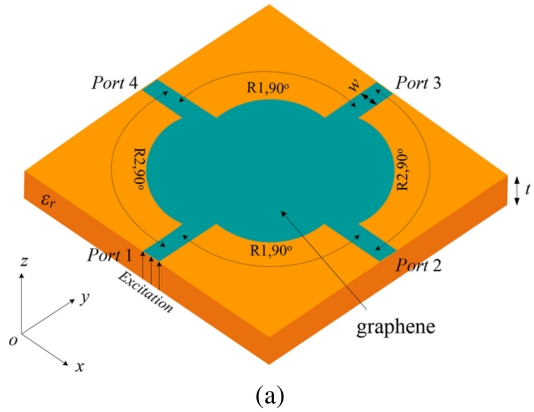

(a)

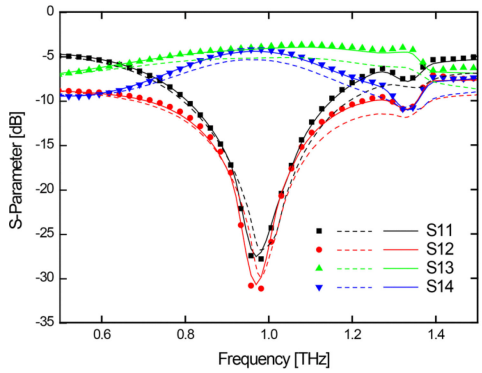

(b)

Fig. 2. (a) Schematic description of the monolayer graphene-based patch coupler. (b) S-parameters of the coupler computed using the conformal HIE-FDTD with coarse mesh (symbols), the staircase HIE-FDTD with coarse mesh (dashed line), and the staircase HIE-FDTD with fine mesh (solid line). Reproduced with permission from [70].

(CFL) stability condition. As a result execution time and memory requirement of the traditional fully explicit FDTD method increases. To alleviate this bottleneck, various unconditionally stable time marching schemes, such as the alternating-direction-implicit (ADI) FDTD method and the locally one-dimensional (LOD) FDTD method, have been developed. These algorithms remove or relax the limitations of the CFL condition. The one-step leapfrog ADI-FDTD method has been applied to simulation of surface plasmon polaritons (SPPs) propagating along a graphene slab biased by an electrostatic field [62] and the LOD-FDTD method has been used to model more complicated graphene devices [63]. Additionally, a matrix exponential FDTD method has been developed to reduce the memory requirements of the traditional FDTD method when applied to fine volumetric grids discretizing a magnetically biased graphene layer [64].

While simulating a very thin structure like graphene using the FDTD method, the computational efficiency is restrained by the finest grid size only in one dimension. Therefore, it is sufficient to use implicit FDTD updates/iterations only in this dimension while keeping them explicit in the remaining two dimensions. This approach increases the efficiency by avoiding unnecessary implicit updates and relaxing the CFL condition for the explicit one in one dimension. To this end, several weakly conditional stable (WCS) FDTD methods have been developed. Examples of these include the WCS-FDTD method [65] and the hybrid implicit–explicit (HIE) FDTD method [66], [67]. Additionally, the HIE-FDTD has been updated to account for dispersive material properties and used in design of a graphene-based absorber [54] and polarizer [68]. Similarly, a graphene-based absorber has also been simulated using the WCS-FDTD method [69].

Furthermore, a conformal version of the HIE-FDTD method has been developed to analyze tunable graphene-based couplers for THz applications [70]. As shown in the inset of Fig. 1, the graphene sheet is located on the xy plane and excited by a planewave polarized along the x-direction. The excitation is introduced in the FDTD method using the total-field/scattered-field (TF/SF) technique. The parameters of graphene are selected as $\mu_c = 0.1$ eV, $T = 300$ K, and $\tau = 1$ ps. The convolution perfectly matched layer (CPML) is used to truncate the unbounded background medium in the z-direction and a periodic boundary condition is enforced along the x and y directions to model an infinitely wide graphene plane.

Fig. 1 plots the transmission coefficient versus frequency as computed using HIE-FDTD, traditional FDTD, and an analytical expression. All results are in good agreement. The execution times required by HIE-FDTD and FDTD are 157 and 613 s, respectively, demonstrating the efficiency of the HIE-FDTD method. Fig. 2(a) provides the schematic description of a graphene-based patch coupler, with its backside being grounded. The dielectric constant and thickness of the substrate are $\varepsilon_r = 2.33$ and $t = 2$ μm, respectively. The width of the graphene strip is $W = 12$ μm, and radii of the circular sector patches are $R_1 = 20$ μm and $R_2 = 25$ μm. The parameters of graphene are $\mu_c = 0.5$ eV, $\Gamma = 0.41$ meV/h, and $T = 300$ K. A vertical electric field is generated by a sinusoid modulated Gaussian pulse in the rectangular region underneath Port 1 along the z-direction. The S-parameters are computed using $[S] = [V]^r/[V]^i$, where $[V]^r$ and $[V]^i$ are the reflected and incident voltage vectors recorded at the ports, respectively. The S-parameters computed using the conformal HIE-FDTD with coarse mesh (symbols), the staircase HIE-FDTD with coarse

mesh (dashed line), and the staircase HIE-FDTD with fine mesh (solid line) (reference results) are shown in Fig. 2(b). The results obtained from the conformal method agree well with the reference results. However, the results of the staircase method with coarse mesh are significantly different than the other two.

As mentioned above, the second approach to modeling graphene using the FDTD requires subcell techniques to be implemented. The subcell FDTD method [55] has been first used in simulation of dispersive thin layers and it has been immediately recognized as an effective way to model graphene [71]. The subcell technique is an efficient approach since a coarse mesh can be still used, and the thin layer only occupies a fraction of the grid. As a result, the memory requirements remain almost unchanged after the insertion of the layer, which fills only a small amount of the computation space. Since two kinds of materials exist in one cell at the same time, this method divides the electric and magnetic components, which are normal to the graphene sheet, into two parts since they are not continuous across the interface. Conversely, tangential components do not require any splitting, due to their continuity across the boundary. Later on, aim at thin dispersive layers that is outstretched to the boundaries of the computational domain, a subcell perfectly matched layer scheme in FDTD is proposed [72].

The third approach represents the graphene sheet as an IBC with zero thickness (instead of conductive volume as done by the first approach) [56], [57]. This approach eliminates the need for a fine discretization/grid in the vicinity of the graphene sheet and alleviates the inefficiency that comes with it due to the CFL condition. The method has been first proposed in [56]. Fig. 3(a) shows a conductive (graphene) sheet positioned on the xy plane that coincides with $K+1/2$ indexed z grid of a 3-D FDTD Yee cell. The discontinuous boundary condition

$$\hat{\mathbf{n}} \times \left[{}^{2}\mathbf{H}\left(\omega\right) - {}^{1}\mathbf{H}\left(\omega\right)\right] = \sigma_d \mathbf{E}_t\left(\omega\right) \tag{5}$$

is enforced on the conductive sheet. Here, $\hat{\mathbf{n}}$ is the unit vector normal to the sheet, ${}^{1}\mathbf{H}$ and ${}^{2}\mathbf{H}$ are the magnetic fields at its two sides, the superscripts 1 and 2 designate the bottom and top sides, respectively. $\mathbf{E}_t$ denotes the component of the electric field tangential to the sheet. The boundary condition in (5) should be transformed into the TD so that it can be used within an FDTD method [56]. To this end, the intraband conductivity is represented using a Drude-like model while the interband conductivity is expressed in terms of complex conjugate pole-residues pairs [57].

Note that the conductive sheet supports electric current and charge, therefore, the tangential component of the magnetic field and the normal component of the electric field is split into two parts that are positioned at the bottom and top sides of the sheet. As a result, the FDTD update equations for ${}^{1}H_x^n$ and ${}^{2}H_x^n$ are obtained as

$$\begin{aligned}\mu_1 \delta_t^c \left\{{}^{1}H_x^n\right\} &= \delta_z^b \left\{E_y^n\left(i, j+1/2, k+1/2\right)\right\} \\ &\quad - \delta_y^c \left\{{}^{1}E_z^n\left(i, j+1/2, k+1/2\right)\right\} \end{aligned} \tag{6}$$

$$\begin{aligned}\mu_2 \delta_t^c \left\{{}^{2}H_x^n\right\} &= \delta_z^f \left\{E_y^n\left(i, j+1/2, k+1/2\right)\right\} \\ &\quad - \delta_y^c \left\{{}^{2}E_z^n\left(i, j+1/2, k+1/2\right)\right\} \end{aligned} \tag{7}$$

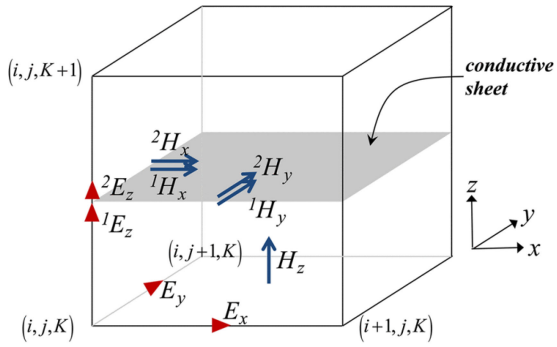

(a)

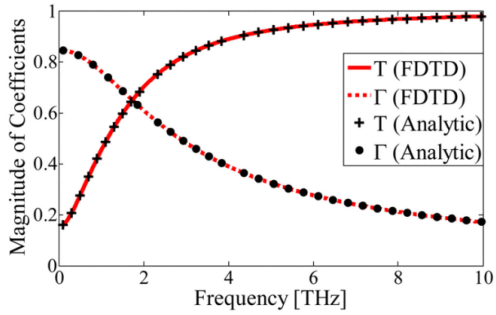

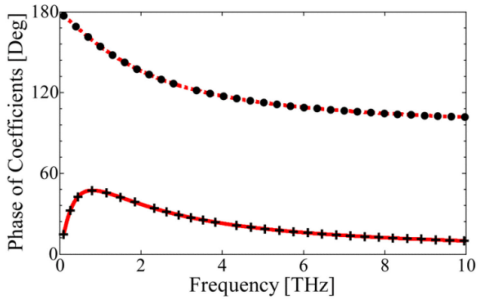

(b)

Fig. 3. (a) FDTD Yee cell enclosing a conductive (graphene) sheet. (b) Magnitude and phase of transmittance (T) and reflectance (Γ) for a planewave on normally incident on the graphene layer. Reproduced with permission from [56].

where μ_1 and μ_2 are the permeabilities of the media at the bottom and top sides of the sheet, δ represents the finite difference operation, the superscripts c, f, and b designate the central, forward, and backward difference, respectively; the subscripts t and x, y, and z designate the derivates in time and along x-, y-, and z-directions, respectively. Similarly, the update equations for ${}^{1}E_z^n$ and ${}^{2}E_z^n$ are derived as

$${}^{1}E_z^{n+1} = {}^{1}E_z^n + \frac{\Delta t}{\varepsilon_1}\left[\delta_x^c\left\{{}^{1}H_y^n\right\} - \delta_y^c\left\{{}^{1}H_x^n\right\}\right] \tag{8}$$

$${}^{2}E_z^{n+1} = {}^{2}E_z^n + \frac{\Delta t}{\varepsilon_2}\left[\delta_x^c\left\{{}^{2}H_y^n\right\} - \delta_y^c\left\{{}^{2}H_x^n\right\}\right] \tag{9}$$

where ε_1 and ε_2 are the permittivities of the media at the bottom and top sides of the sheet. It should be mentioned here that the conductive surface boundary condition reviewed previously has been extended to account for anistropic modeling of graphene sheets. The resulting boundary conditions have been

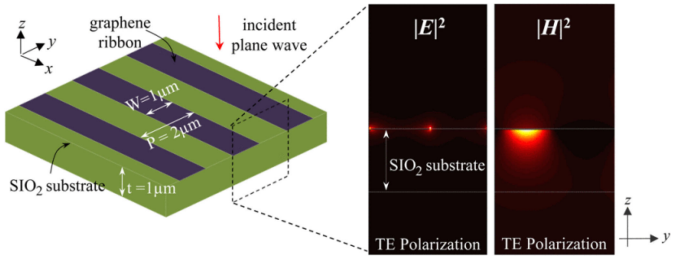

Fig. 4. (a) Schematic description of the periodic graphene microribbon array supported by a SIO_2 thin film and the planewave normally incident on it. (b) Intensities of the electric and magnetic fields long after the TE polarized planewave pulse has passed the array. Reproduced with permission from [56].

used within FDTD to simulate EM interactions on magnetized graphene [73].

Fig. 3(b) plots the magnitude and phase of transmittance (T) and reflectance (Γ) computed by the FDTD (with resistive surface boundary condition as briefly explained previously) for a plane wave normally incident on the graphene layer. The figure shows that the FDTD results agree well with those obtained using an analytical method.

At last, a periodic graphene microribbon array has been simulated using the FDTD method with resistive surface boundary condition. The graphene array, which is assumed to extend to infinity along the x-direction and periodically repeated along the y-direction, is shown in Fig. 4(a). A TE-polarized (electric field parallel to the y-direction) or TM-polarized (electric field parallel to the x-direction) planewave is normally incident on the structure. Fig. 5(a) plots the transmission through the structure for plane wave excitations with TE and TM polarizations. For TE polarization, a resonance peak is observed around 8.35 THz. This resonance is a result of the SPPs generated on the structure; the electric and magnetic field intensities at this resonance frequency are demonstrated in Fig. 4(b). The snapshot clearly shows that the effects of the SPP are still observed long after the TE polarized planewave pulse has passed the array. It should be noted here that the array can be used as a polarizer at this frequency. Fig. 5(b) shows that the transmission of the graphene microribbon array resembles that of an infinite graphene sheet for the planewave with TM polarization.

In summary, the FDTD-based approach that assumes zero thickness for the graphene sheet and models it as an IBC is often considered as the most effective one among the three types of FDTD methods reviewed in this section. This is simply because it avoids the very fine volumetric discretization of the graphene layer. Additionally, this approach uses an explicit time marching scheme, which does not call for matrix solutions, further reducing the computation time and memory imprint (in comparison to unconditionally or weakly stable time marching schemes). It should also be noted here that the subcell FDTD scheme also uses a coarse mesh in the vicinity of the graphene layer, but underlying formulation developed to implement two different materials coexisting in one cell "destroys" the simplicity of the FDTD schemes, which makes them attractive in the first place.

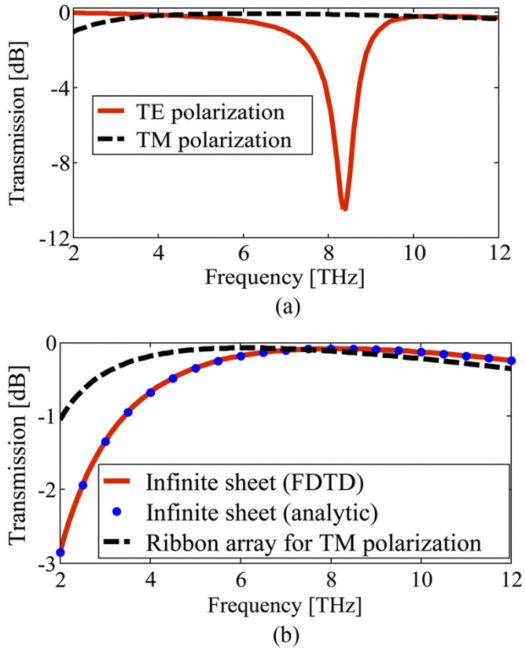

Fig. 5. (a) Transmission through the graphene microribbon array for TE- and TM-polarized normally incident plane waves. (b) Transmission through the graphene microribbon array and infinite sheet computed using the FDTD for TM-polarized normally incident plane wave. Those are compared to transmission through the infinite sheet computed analytically. Reproduced with permission from [56].

C. Finite Element Method

FEM is a powerful and versatile technique for numerically solving boundary-value problems. It treats equations and boundary conditions in a systematic and mathematically rigorous way allowing for straightforward implementation of general-purpose computer programs for solving a wide range of engineering problems. Unlike finite-difference based methods (such as FDTD as described in the previous section), it uses arbitrary meshes (for example, with tetrahedral, hexahedral, or prism elements) to discretize computation domains involving geometrically complex structures with potentially inhomogeneous material properties [74]. There are the following four basic steps involved in the finite element analysis:

1) discretize the computation domain into a finite number of nonoverlapping elements;
2) select a proper set of basis/interpolation functions to expand unknown variables;
3) formulate a system of equations using Ritz variational or Galerkin method;
4) solve the resulting system of equations.

Several successful commercial software making use of FEM has been developed in the last several decades as it has become a maturing numerical tool widely used in the field of electromagnetics. Three very well-known examples of such commercial software are CST MICROWAVE STUDIO [75], COMSOL [76], and high-frequency structure simulator [77]. A plethora of examples on the use of these softwares for analyzing electromagnetic field/wave interactions on graphene exist in the literature. Please

see [78]–[82] for some of those. It should be noted here that in the application of these commercial software to the EM simulation of graphene, graphene sheet is often modeled as any other material, i.e., as a finite-thickness layer with a certain volumetric conductivity value. To alleviate the increased computational requirements that come with this approach, techniques relying on impedance transmission boundary condition (ITBC) [83] and impedance network boundary condition (INBC) [84] to model thin layers of graphene have been into FEM.

It should also be noted here that the approaches and commercial tools mentioned above rely on FD-FEM that directly works with conductivity values of graphene at the frequency of interest. For an FEM operating in TD (i.e., TD-FEM), the dispersive conductivity expression has to be converted into TD, just like it is done with FDTD. But note that the reason why TD-FEM is not the first method of choice for transient EM simulations of graphene is the fact that it requires the inversion of a sparse matrix system at every time step. This can be avoided using DGTD as described in the following section.

D. Discontinuous Galerkin Time-Domain Method

The DGTD method [85]–[87] combines the advantages of the finite-volume method (FVM) [88] and FEM and it has been successfully applied in various fields of computational sciences, engineering, and physics for solving different PDEs. Like FEM, the discretization of the computation domain can be done using an arbitrary mesh and high-order accuracy convergence can be obtained using high-order basis functions. Like FVM, all spatial DGTD operations are localized since numerical flux is enforced on the surface of a given discretization element to "realize" information flow from/to its neighboring elements. This localization translates into a global mass matrix being divided into block-diagonal mass matrices. The inversion and storage of these mass-matrix blocks (as would be constructed by the finite element TD method [89]) are carried out before the time marching starts. This renders the resulting DGTD-based solver very compact (efficient with a very small memory imprint) especially when an explicit integration method is used for time marching. Additionally, the use of numerical flux and the resulting spatial localization allow for nonconformal meshes to discretize the computation domain and make it easy to implement adaptive h and/or p refinement schemes and parallelization on distributed memory computer clusters. Because of the properties listed previously, the DGTD is the natural method of choice for multiscale electromagnetic simulations involving thin sheets of graphene.

The approach, which makes use of resistive boundary condition (RBC) and is originally developed for the FDTD method, can also be implemented within the DGTD method for efficient simulation of graphene sheets [90]. This implementation can be summarized as follows: First a numerical flux, which takes into account the fields satisfying the RBC, is reformulated from the Rankine–Hugoniot condition [90]. The conductivity of graphene is approximated as a summation of rational functions (of frequency) using the fast-relaxation vector-fitting method [91]. Then, applying inverse Laplace transform to this summation, the corresponding TD matrix equations are obtained. These equations are solved using the TD finite integral technique. For elements not touching the graphene sheet, however, the well-known Runge–Kutta (RK) method is employed to solve the two first-order time-derivative Maxwell equations as done with a "traditional" DGTD method.

This RBC-enhanced DGTD scheme is further improved for electromagnetic numerical characterization of magnetically biased graphene that has an anisotropic and dispersive surface conductivity (caused by Lorentz force). This improvement makes use of an auxiliary surface polarization current governed by a first-order time-dependent partial differential equation (PDE) that is enforced on the graphene, and is instrumental in obtaining an isotropic and simultaneously nondispersive RBC. As a consequence, a numerical flux, which is isotropic and does not call for temporal convolution computations during the solution of the final system of equations, is obtained. The applicability and accuracy of the this method are demonstrated through its application to the transient simulation of magnetized graphene for a wideband changing from microwave to THz frequencies [92]. These simulations are briefly described as follows.

For the first example, an infinitely large graphene sheet located on the xy plane is biased by a z-directed magnetostatic field $\mathbf{B}_0 = \widehat{\mathbf{z}} B_0$. The chemical potential and scattering time are set as $\mu_c = 0.5$ eV and $\tau = 5 \times 10^{-12}$ s, while the magnetic biasing amplitude B_0 is changed in the range [0.5, 30] T. Fig. 6(a) and (b) plots the total transmission coefficient and the Faraday rotation angle obtained using DGTD and compare them to those computed by analytical methods. Additionally, the cross-polarized transmission coefficient obtained using DGTD is provided in Fig. 6(c). These results demonstrate that the behavior of an electromagnetic wave propagating through a graphene sheet is clearly influenced by the magnetostatic biasing.

For the second example, first an unmagnetized graphene patch is simulated using the DGTD scheme to further verify the accuracy via comparison of the results with those obtained by an IE solver (see Section II-E). Fig. 7(a) plots the extinction cross-section (ECS) computed by these two methods: the results agree well. It should be noted here that, the DGTD method uses the TD boundary integral algorithm to accurately truncate the computation domain. Then, the same graphene patch is simulated again but this time under a z-directed biasing (static) magnetic field $B_0 = 0.25$ T. Fig. 7(b) and (c), respectively, plots the total scattering-cross-section (TSCS) and ECS for different values of the chemical potential μ_c, demonstrating the effects of the plasmon resonances on the scattering characteristics of the graphene patch. It can be concluded that the plasmon resonance becomes stronger and its frequency has a blue shift as the chemical potential is increased. Furthermore, the effect of the substrate on the plasmon resonance is investigated using the DGTD method. Three materials are considered as the substrate of the graphene patch (with $\mu_c = 0.5$ eV): silicon (Si) with $\varepsilon_r = 4.0$, silicon-dioxide (SiO_2) with $\varepsilon_r = 7.0$, and silicon-nitrate (Si_3N_4) with $\varepsilon_r = 11.9$. Normalized ECS of the graphene patch for different types of substrate is shown in Fig. 7(d). The

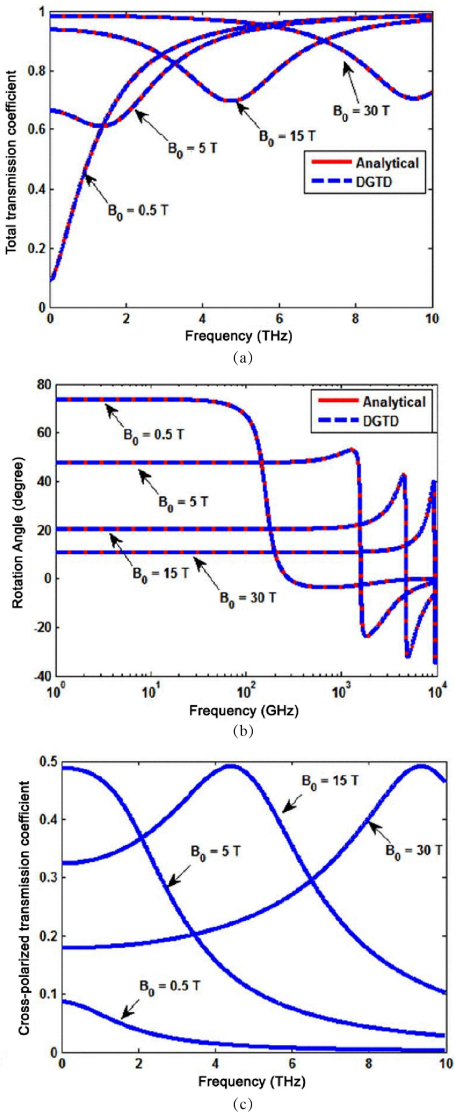

Fig. 6. (a) Total transmission coefficients. (b) Faraday rotation angle computed using DGTD and analytical expressions for different bias field amplitudes. (c) Cross-polarized transmission coefficient computed using DGTD for different bias field amplitudes. Reproduced with permission from [92].

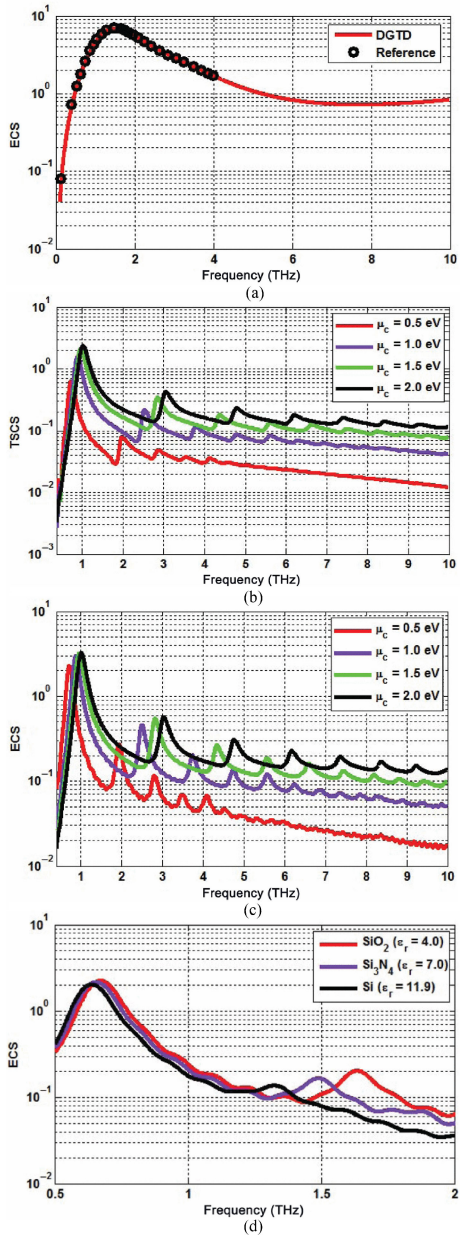

Fig. 7. (a) ECS of the unbiased graphene patch computed using the DGTD and the IE solvers. (b) Normalized TSCS and (c) ECS computed using the DGTD for different values of chemical potential. (d) Normalized ECS for substrates Si, SiO_2, and Si_3N_4. Reproduced with permission from [92].

figure shows that a red shift happens at the first two peaks of the plasmon resonance as the permittivity of the substrate is increased. This can be explained by the fact that an increase in permittivity effectively increases the dimension of the graphene in terms of wavelength.

Furthermore, to account for spatial dispersion effects associated with graphene [which are observed when its conductivity is modeled as nonlocal and a function of spectral wavenumber (momentum operator) q], a nonlocal transparent surface impedance boundary condition (SIBC) has been incorporated into the DGTD method. Since there is no exact TD SIBC that can be utilized to model the complex conductivity, which is now a function of q, it is approximated using a Taylor series expansion in spectral domain under the low-q assumption. This facilitates the formulation of a second-order PDE in electric field and current density that is solved together with Maxwell equations using the DGTD method. The nonlocal properties of GNRs have been simulated by this DGTD framework [22].

In addition to RBC and SIBC, in [93], the ITBC has been used within a wave-equation-based DGTD with the same purpose of avoiding a very fine mesh around and inside the graphene layer.

E. Method of Moments

MoM [94] is a numerical technique that is used to solve surface integral equations (SIEs) by converting them into a linear matrix system of equations as briefly explained next:

Using equivalence principle, the scatterers consisting of dielectric/perfect electrically conducting bodies are "effectively" replaced by equivalent electric and magnetic current densities introduced on their surfaces. Then, the scattered fields are represented as convolutions of these unknown current densities and the Green functions of the unbounded media with the material properties of the background and/or the dielectric bodies. SIEs in these unknown current densities are constructed on the interfaces using boundary conditions on the total (incident plus scattered) electric and magnetic fields. Unknown current densities are expanded using basis functions. Inserting these expansions into the SIEs and testing the resulting equation (for example, using Galerkin scheme) yield the MOM matrix equation. The SIE solvers have several advantages over Maxwell equation solvers (such as FEM): They only discretize the surface of the scatterers, effectively reducing the dimension of the problem from three to two. They implicitly enforce the radiation condition therefore do not call for approximate methods to truncate (unbounded) physical domains into computation domains. One disadvantage of the SIE solvers is that the matrix resulting from the discretization of the SIE is dense, which increases the computational cost of the matrix solution. However, with the development of fast solvers (such as multilevel fast multipole method (MLFMM) [95] and adaptive integral method (AIM) [96], this bottleneck is no longer prohibitive in solving large-scale practical problems. Consequently, SIE solvers have become prime candidates for simulating graphene-based electromagnetic devices and systems.

In [98], the SIBC associated with the graphene is cooperated into SIEs and the resulting set of equations are solving using the Nyström method. The simulation of graphene strips, which is carried out using this method, shows that the surface plasmon resonances can be tailored by tuning the chemical potential and relaxation times of graphene [98]. Then, a further discussion of THz wave scattering from graphene strips and disks is presented to demonstrate that the chemical potential of graphene can adjust the wavelength of plasmon resonance in the THz waveband [99]. Furthermore in [100] and [101], the properties of GNRs are analyzed using another SIE solver.

Another method that has been developed to model graphene within SIE solvers assumes that it has a finite thickness of 0.5 nm [97]. Then, an SIE solver, which uses a multilayered medium Green function (instead of the unbounded medium Green function as explained at the beginning of this section) is used to simulate the structure shown in Fig. 8. This structure involves a split-ring resonator (SRR) embedded in a layer of ZnO and a graphene layer located between the ZnO layer and a layer of a SiO_2 substrate. The dimensions of the SRR are optimized to make sure that the graphene plasmonics and metallic plasmonics overlap in the same part of the frequency spectrum. In the first set of simulations, graphene layer is removed and Fig. 9(a) demonstrates that only the x-oriented dipole source can "couple" to the SRR as shown by the photon decay rate. It can be seen from Fig. 9(b) that the position of the source only affects the amplitude of the decay rate's peak but has no effect on its frequency. In the second set of simulations, the graphene layer is introduced into the system. As shown by Fig. 9(c), the amplitude of the photon decay rate is enhanced especially in the proximity of the graphene layer. The dependence of the decay rate on the chemical potential of the graphene is shown in Fig. 9(d). The photon decay rate is not only blue-shifted but also splits into several peaks due to a strong coupling between the SRR and the graphene.

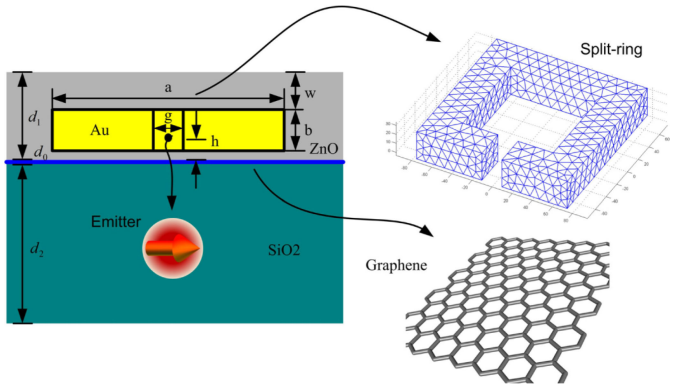

Fig. 8. Schematic configuration of a complicated electromagnetic system for manipulating photon decay rates. Reproduced with permission from [97], Copyright The Optical Society, 2015.

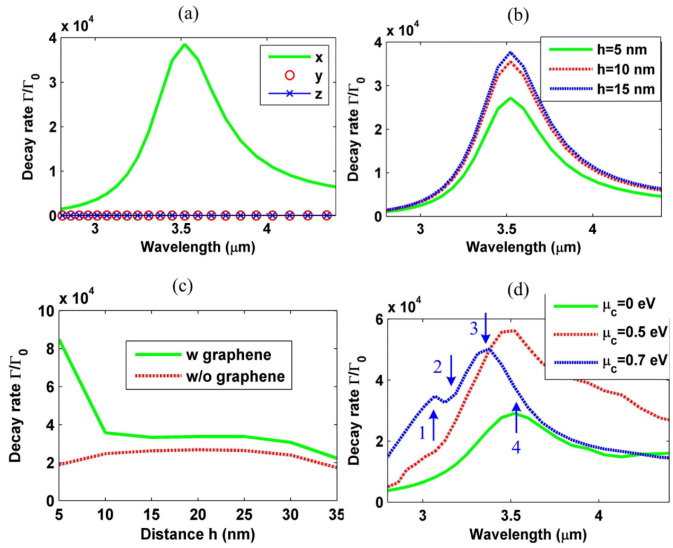

Fig. 9. (a) Polarization effect of a dipole at the center of the resonator gap without a graphene layer. (b) Position effect of a x-oriented dipole inside the resonator gap without a graphene layer. (c) Position effect of a x-oriented dipole with and without a graphene layer. (d) Chemical potential effect of a x-oriented dipole in the hybrid system. Reproduced with permission from [97], Copyright The Optical Society, 2015.

Furthermore, in [102], a marching-on-in-time (MOT) scheme has been developed to solve TD SIEs enforced on interfaces of a graphene-based devices. In addition, in [103], graphene layer has been modeled as a thin dielectric sheet (TDS) (with dispersive conductivity) within an MOT solver. This approach "converts" the TD volume integral equation (TD-VIE) equation into a TD-SIE and eliminates the need for a very fine volumetric mesh inside the graphene layer. These MOT solvers methods can be thought as TD MoM.

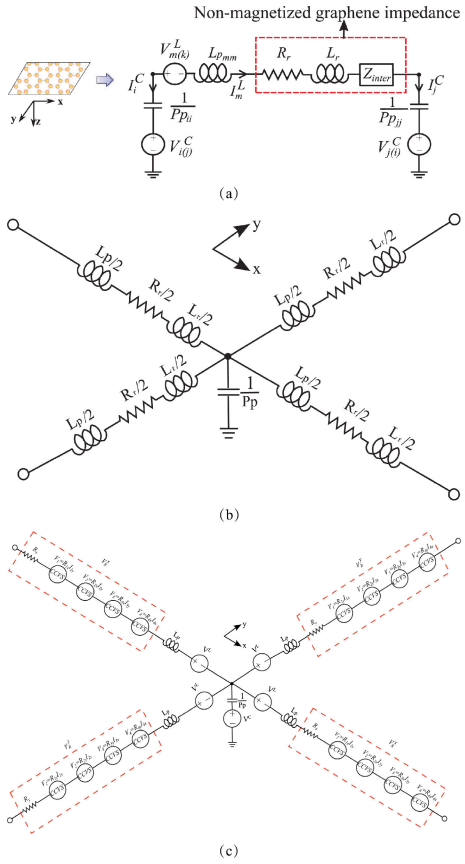

Fig. 10. (a) One-cell PEEC model for a nonmagnetized graphene patch. (b) Unit model for uniform PEEC cell of nonmagnetized graphene. (c) Complete equivalent circuit for anisotropic graphene. Reproduced with permission from [105] and [106].

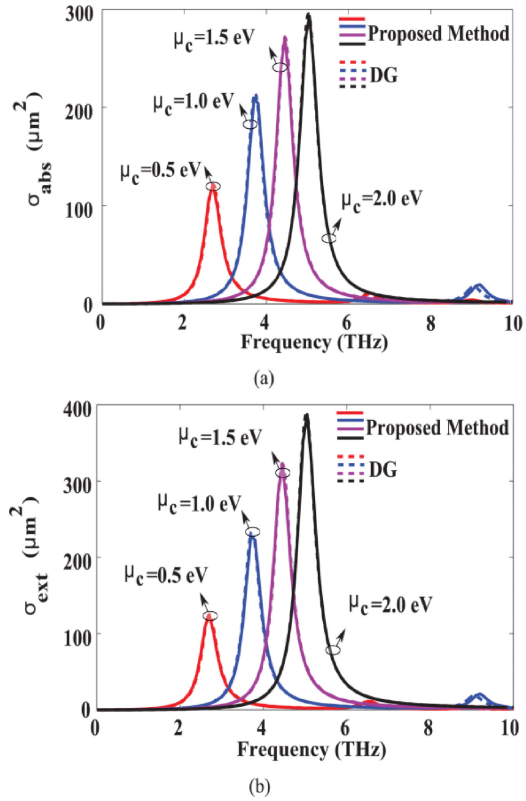

Fig. 11. Comparison of (a) σ_{abs} (absorption cross section) and (b) σ_{ext} (ECS) of the graphene patch simulated with the PEEC method [106] and the DGTD method [92]. Reproduced with permission from [106].

F. Partial Element Equivalent Circuit (PEEC) Method

The PEEC method [104], which is developed using potential-based volume integral equation formulations and the charge-current continuity equation, has often been used in electromagnetic simulation of ICs. However, with recently increasing interest in graphene-based devices, it has been improved to take into account graphene sheets.

To this end, a surface conductivity circuit model consisting of a resistor, an inductor, and an impedance element is introduced into the PEEC method to efficiently characterize graphene [105]. This is effectively equivalent to enforcing an IBC on the graphene surface. Fig. 10(a) illustrates one-cell of the PEEC model for the graphene patch, the circuit elements inside the red rectangle approximate the nonmagnetized graphene's impedance caused by the conduction loss. The resistance R_r and inductance L_r represent the intraband contribution while the complex impedance Z_{inter} corresponds to the interband contribution. $V^L_{m(k)}$ is the voltage source representing the external electric field, $V^C_{i(j)}$ and $V^C_{j(i)}$ are the voltage control voltage sources (VCVSs), $P_{p_{mm}}$ and $P_{p_{m+1,m+1}}$ are the potential self-coefficients for the circuit model. Fig. 10(b) demonstrates the PEEC circuit model for the nonmagnetized graphene patch. It shows that there are four current filaments sharing the same common node in the PEEC partition and each branch is a simplification of the circuit given in Fig. 10(a). To model the anisotropy of graphene under a magnetostatic bias, the resistive part of the unit circuit is replaced by a resistor in series with current-controlled voltage sources [106]. The complete equivalent circuit which combines x- and y-directional resistive cell for anisotropic graphene is sketched in Fig. 10(c).

In [106], PEEC is used to simulate EM interactions on a magnetized graphene patch of dimensions $10 \times 2\,\mu\text{m}^2$. The graphene patch is illuminated by plane wave propagating the z-direction and linearly polarized along the length of the patch. Biasing static magnetic field is z directed with an amplitude of 0.25 T. In Fig. 11(a), the σ_{abs} (absorption cross section) and (b) σ_{ext} (ECS) of the magnetized graphene patch computed using PEEC [106] and DGTD [92]. The results are in good agreement validating the accuracy of these two methods.

Furthermore, in [107], a TD solver making use of the PEEC model has been developed for wideband electromagnetic simulations of graphene-based devices.

III. Summary and Comparison

Section II gives a rather detailed review of numerical tools developed for simulation of EM interactions on graphene sheets and graphene-based devices. In this section, the important points of this review are summarized.

A. Summary of IBCs

To this date, following three main groups of IBC formulations have been developed to model to thin layers of materials: 1) SIBC (which is also termed SBC [56] or RBC [92]), 2) ITBC [83], and 3) INBC [84].

The SIBC is formulated under the assumption that the variation of the fields inside the thin conductor layer is linear and larger than the variation of the fields along its surface. As a result, the SIBC technique requires that the layer thickness to be smaller than the skin depth inside the layer. As detailed in the article, this technique has been successfully used to model graphene sheets within FDTD, DGTD, MOT, and PEEC methods at the THz frequency band. For lower frequencies, the graphene layer's thickness becomes larger than the skin depth, and therefore, it becomes almost transparent to the electromagnetic fields [83]. For such cases, the ITBC formulation, which is derived using the transmission line theory, is more suitable to model the tangential electromagnetic fields on both sides of the graphene surface. The INBC technique, which describes the field inside a conductive sheet using two-port network equations, has a wider range of applicability in modeling good conductor layers (i.e., $\sigma \gg \omega\varepsilon$) than the SIBC and the ITBC since it is not restricted by the skin depth.

B. Methods for EM Simulation Graphene

FD methods can directly use conductivity values of graphene obtained via experiments or calculated using the mathematical expression at the frequency of interest. But they are limited to single-frequency or narrow-band problems. From this perspective, TD methods have an advantage over FD methods since they can produce broadband results with a single execution of the simulation. However, since the graphene's conductivity is dispersive, it has to be "converted" into TD using the Drude model or some variation of "vector fitting" schemes. Both FD and TD methods can benefit from IBC-based techniques to avoid generation of a very fine mesh around and inside the graphene layer.

FDTD and PEEC, by design, use orthogonal grids to discretize the geometries and Maxwell equations. This leads to additional staircase approximation errors, when they are used in analyzing graphene based devices with curved surfaces. On the other hand, FEM (both FD and TD versions), DGTD, MoM, and MOT, which use triangular and/or tetrahedral elements, can account of arbitrary geometries more accurately. Even though the SIE formulation used by MoM and MOT reduces the dimension of the problem from three to two (from volume to surface modeling), their computational requirements increase significantly for electrically large devices. In this case, one has to use a fast solver, such as MLFMM [95] and AIM [108] in FD and plane-wave TD method [109] and TD-AIM [96] in TD.

In short, for simulating EM interactions on graphene sheets and graphene based devices, one often chooses FEM and DGTD for their ability to model arbitrary geometries, which helps with increasing the accuracy of the solution and the FDTD due to its simplicity that eases the burden of implementation.

IV. Future Research Directions

In many EM applications that benefit from graphene's electrical properties, device sizes are getting smaller at nano-scales and optical operation frequencies are becoming the norm. In such scenarios, a rather simplified graphene conductivity model as revised in this article may not be accurate enough. For example, at lower frequencies where, traditional integrated circuits (ICs) are operated, both photon and thermal excitation energies of graphene are much weaker than its Fermi energy; therefore, the intraband transitions become dominant over interband transitions. As a result, a simplified steady-state model making use of the intraband contribution in Kubo formula is commonly used to describe graphene's conductivity. This Drude-type model is from the Boltzmann transport equation and the Ohm law under several assumptions. However, it has been recently reported that for high-frequency simulation of Cu-G hybrid nano-interconnects (which are orders of magnitude smaller than regular interconnects), this model is not accurate [110], [111]. This is because graphene's skin depth becomes comparable to its mean free path, the carriers are no longer influenced by a constant field between collisions, and the current at a given point also depends on the electric field at other points. To address this challenge, in [110] and [111], a first-principles-based solver has been developed to solve a coupled system of Maxwell and Boltzman equations to characterize EM interactions on graphene. This solver provides more accurate results as compared to the numerical scheme that account for graphene with an effective conductivity model. It is worth mentioning here that this approach is fully aligned with recent research directions in other branches of computational sciences where development of multiphysics and multiscale simulations are deemed important.

Another challenging direction is to develop numerical schemes that can accurately account for the nonlinearity of graphene's susceptibility. This is especially important with graphene becoming a building block in plasmonic device design. In such designs, highly localized and strong EM fields "activate" the nonlinear response of the graphene. For example, in [112], a graphene metasurface has been studied using FDTD that accounts for the nonlinear susceptibility effects using a homogenization scheme. In [29], Maxwell equations are complemented by a nonlinear auxiliary equation (describing current-field relationship on graphene sheet), and this coupled system is solved using FDTD to analyze EM/plasmonic interactions on a nanoantenna with the metal-insulator-graphene configuration. In [113] and [114], the nonlinear properties of graphene is studied again using FDTD, which is developed based on the quasi-classical (Boltzmann) approach [115], [116].

V. Conclusion

In the last decade, graphene's excellent electrical and mechanical properties have made it a focus of significant research interest. A scientific literature has been flooded with theoretical studies of graphene's properties and the physical mechanism behind those as well as investigations of its practical use in various fields of engineering.

In this article, we review a few of the most popular numerical algorithms from the research field of CEM and some of their recent adaptations formulated and implemented for efficient and accurate simulation of graphene-based devices.

REFERENCES

[1] K. S. Novoselov *et al.*, "Electric field effect in atomically thin carbon films," *Science*, vol. 306, no. 5696, pp. 666–669, Oct. 2004.

[2] K. S. Novoselov *et al.*, "A roadmap for graphene," *Nature*, vol. 490, no. 7419, pp. 192–200, Oct. 2012.

[3] A. C. Neto, F. Guinea, N. M. Peres, K. S. Novoselov, and A. K. Geim, "The electronic properties of graphene," *Rev. Mod. Phys.*, vol. 81, no. 1, pp. 109–162, Jan. 2009.

[4] P. Blake *et al.*, "Graphene-based liquid crystal device," *Nano Lett.*, vol. 8, no. 6, pp. 1704–1708, Apr. 2008.

[5] K. S. Novoselov *et al.*, "Room-temperature quantum Hall effect in graphene," *Science*, vol. 315, no. 5817, pp. 1379–1379, Mar. 2007.

[6] F. Bonaccorso, Z. Sun, T. Hasan, and A. Ferrari, "Graphene photonics and optoelectronics," *Nature Photon.*, vol. 4, no. 9, pp. 611–622, Aug. 2010.

[7] P. R. Wallace, "The band theory of graphite," *Phys. Rev.*, vol. 71, no. 9, pp. 622–634, May 1947.

[8] K. S. Novoselov *et al.*, "Two-dimensional atomic crystals," *Proc. Nat. Acad. Sci. USA*, vol. 102, no. 30, pp. 10 451–10 453, Jul. 2005.

[9] K. S. Novoselov, A. Mishchenko, A. Carvalho, and A. C. Neto, "2D materials and van der Waals heterostructures," *Science*, vol. 353, no. 6298, Jul. 2016, Art. no. aac9439.

[10] L. Song *et al.*, "Large scale growth and characterization of atomic hexagonal boron nitride layers," *Nano Lett.*, vol. 10, no. 8, pp. 3209–3215, Jul. 2010.

[11] L. Li *et al.*, "Black phosphorus field-effect transistors," *Nature Nanotechnol.*, vol. 9, no. 5, pp. 372–377, Mar. 2014.

[12] X. Xi *et al.*, "Strongly enhanced charge-density-wave order in monolayer $NbSe_2$," *Nature Nanotechnol.*, vol. 10, no. 9, pp. 765–769, Jul. 2015.

[13] L. Britnell *et al.*, "Resonant tunnelling and negative differential conductance in graphene transistors," *Nature Commun.*, vol. 4, Apr. 2013, Art. no. 1794.

[14] F. Xia, H. Yan, and P. Avouris, "The interaction of light and graphene: Basics, devices, and applications," *Proc. IEEE*, vol. 101, no. 7, pp. 1717–1731, Jul. 2013.

[15] K. F. Mak, L. Ju, F. Wang, and T. F. Heinz, "Optical spectroscopy of graphene: From the far infrared to the ultraviolet," *Sol. State Commun.*, vol. 152, no. 15, pp. 1341–1349, Aug. 2012.

[16] Y. Zhang, Y.-W. Tan, H. L. Stormer, and P. Kim, "Experimental observation of the quantum Hall effect and Berry's phase in graphene," *Nature*, vol. 438, no. 7065, pp. 201–204, Nov. 2005.

[17] P. Avouris, "Graphene: Electronic and photonic properties and devices," *Nano Lett.*, vol. 10, no. 11, pp. 4285–4294, Sep. 2010.

[18] A. Grigorenko, M. Polini, and K. Novoselov, "Graphene plasmonics," *Nature Photon.*, vol. 6, no. 11, pp. 749–758, Nov. 2012.

[19] L. Ju *et al.*, "Graphene plasmonics for tunable terahertz metamaterials," *Nature Nanotechnol.*, vol. 6, no. 10, pp. 630–634, Sep. 2011.

[20] M. Liu *et al.*, "A graphene-based broadband optical modulator," *Nature*, vol. 474, no. 7349, pp. 64–67, May 2011.

[21] F. Schwierz "Graphene transistors," *Nature Nanotechnol.*, vol. 5, no. 7, pp. 487–496, May 2010.

[22] P. Li, L. J. Jiang, and H. Bagci, "Discontinuous Galerkin time-domain modeling of graphene nano-ribbon incorporating the spatial dispersion effects," *IEEE Trans. Antennas Propag.*, vol. 66, no. 7, pp. 3590–3598, Jul. 2018.

[23] E. V. Castro *et al.*, "Biased bilayer graphene: Semiconductor with a gap tunable by the electric field effect," *Phys. Rev. Lett.*, vol. 99, no. 21, Nov. 2007, Art. no. 216802.

[24] L. Ponomarenko *et al.*, "Chaotic Dirac billiard in graphene quantum dots," *Science*, vol. 320, no. 5874, pp. 356–358, Apr. 2008.

[25] M. C. Lemme, T. J. Echtermeyer, M. Baus, and H. Kurz, "A graphene field-effect device," *IEEE Electron Device Lett.*, vol. 28, no. 4, pp. 282–284, Apr. 2007.

[26] J. Wu *et al.*, "Organic light-emitting diodes on solution-processed graphene transparent electrodes," *ACS Nano*, vol. 4, no. 1, pp. 43–48, Nov. 2009.

[27] Z. Yin *et al.*, "Graphene-based materials for solar cell applications," *Adv. Energy Mater.*, vol. 4, no. 1, Sep. 2014, Art. no. 1300574.

[28] P.-Y. Chen, C. Argyropoulos, and A. Alu, "Terahertz antenna phase shifters using integrally-gated graphene transmission-lines," *IEEE Trans. Antennas Propag.*, vol. 61, no. 4, pp. 1528–1537, Apr. 2012.

[29] X. Ren, W. E. Sha, and W. C. Choy, "Tuning optical responses of metallic dipole nanoantenna using graphene," *Opt. Express*, vol. 21, no. 26, pp. 31824–31829, Dec. 2013.

[30] H. Wang, D. Nezich, J. Kong, and T. Palacios, "Graphene frequency multipliers," *IEEE Electron Device Lett.*, vol. 30, no. 5, pp. 547–549, May 2009.

[31] V. Gusynin, S. Sharapov, and J. Carbotte, "Magneto-optical conductivity in graphene," *J. Phys.: Condens. Matter*, vol. 19, no. 2, Dec. 2006, Art. no. 026222.

[32] L. Falkovsky and A. Varlamov, "Space-time dispersion of graphene conductivity," *Eur. Phys. J. B*, vol. 56, no. 4, pp. 281–284, May 2007.

[33] G. W. Hanson, "Dyadic Green's functions and guided surface waves for a surface conductivity model of graphene," *J. App. Phy.*, vol. 103, no. 6, Apr. 2008, Art. no. 064302.

[34] G. W. Hanson, "Dyadic Green's functions for an anisotropic, non-local model of biased graphene," *IEEE Trans. Antennas Propag.*, vol. 56, no. 3, pp. 747–757, Mar. 2008.

[35] Y. Shao, J. J. Yang, and M. Huang, "A review of computational electromagnetic methods for graphene modeling," *Int. J. Antennas Propag.*, vol. 2016, Apr. 2016, Art. no. 7478621.

[36] D. R. Cooper *et al.*, "Experimental review of graphene," *ISRN Condens. Matter Phys.*, vol. 2012, 2012, Art. no. 501686.

[37] M. J. Allen, V. C. Tung, and R. B. Kaner, "Honeycomb carbon: A review of graphene," *Chem. Rev.*, vol. 110, no. 1, pp. 132–145, Jul. 2009.

[38] K. Novoselov, "Nobel lecture: Graphene: Materials in the flatland," *Rev. Mod. Phys.*, vol. 83, no. 3, p. 837, Aug. 2011.

[39] R. Wang, X.-G. Ren, Z. Yan, L.-J. Jiang, W. E. Sha, and G.-C. Shan, "Graphene based functional devices: A short review," *Front. Phys.*, vol. 14, no. 1, Oct. 2019, Art. no. 13603.

[40] A. Crépieux and P. Bruno, "Theory of the anomalous hall effect from the Kubo formula and the dirac equation," *Phys. Rev. B*, vol. 64, no. 1, Jun. 2001, Art. no. 014416.

[41] B. Sensale-Rodriguez *et al.*, "Broadband graphene terahertz modulators enabled by intraband transitions," *Nature Commun.*, vol. 3, no. 1, pp. 1–7, Apr. 2012.

[42] L. Falkovsky and S. Pershoguba, "Optical far-infrared properties of a graphene monolayer and multilayer," *Phys. Rev. B*, vol. 76, no. 15, Oct. 2007, Art. no. 153410.

[43] A. Ferreira, J. Viana-Gomes, J. Nilsson, E. R. Mucciolo, N. M. Peres, and A. C. Neto, "Unified description of the dc conductivity of monolayer and bilayer graphene at finite densities based on resonant scatterers," *Phys. Rev. B*, vol. 83, no. 16, Apr. 2011, Art. no. 165402.

[44] M. Koshino and T. Ando, "Magneto-optical properties of multilayer graphene," *Phys. Rev. B*, vol. 77, no. 11, Mar. 2008, Art. no. 115313.

[45] V. Gusynin, S. Sharapov, and J. Carbotte, "Sum rules for the optical and Hall conductivity in graphene," *Phys. Rev. B*, vol. 75, no. 16, Apr. 2007, Art. no. 165407.

[46] V. Gusynin, S. Sharapov, and J. Carbotte, "Unusual microwave response of Dirac quasiparticles in graphene," *Phys. Rev. Lett.*, vol. 96, no. 25, Jun. 2006, Art. no. 256802.

[47] V. Gusynin and S. Sharapov, "Transport of Dirac quasiparticles in graphene: Hall and optical conductivities," *Phys. Rev. B*, vol. 73, no. 24, Jun. 2006, Art. no. 245411.

[48] A. Mock, "Padé approximant spectral fit for FDTD simulation of graphene in the near infrared," *Opt. Mater. Express*, vol. 2, no. 6, pp. 771–781, Jun. 2012.

[49] E. Levy, "Complex-curve fitting," *IRE Trans. Autom. Control*, no. 1, pp. 37–43, May 1959.

[50] M. Han, R. W. Dutton, and S. Fan, "Model dispersive media in finite-difference time-domain method with complex-conjugate pole-residue pairs," *IEEE Microw. Wireless Compon. Lett.*, vol. 16, no. 3, pp. 119–121, Mar. 2006.

[51] K. Yee, "Numerical solution of initial boundary value problems involving Maxwell's equations in isotropic media," *IEEE Trans. Antennas Propag.*, vol. 14, no. 3, pp. 302–307, May 1966.

[52] K. Niu, Z. Huang, M. Fang, M. Li, X. Li, and X. Wu, "Coupling of gain medium and extraordinary optical transmission for effective loss compensation," *IEEE Access*, vol. 6, pp. 14 820–14 826, 2018.

[53] K. Niu *et al.*, "Linear and nonlinear spin-orbital coupling in golden-angle spiral quasicrystals," *Opt. Express*, vol. 28, no. 1, pp. 334–344, Jan. 2020.

[54] J. Chen, J. Li, and Q. H. Liu, "Designing graphene-based absorber by using HIE-FDTD method," *IEEE Trans. Antennas Propag.*, vol. 65, no. 4, pp. 1896–1902, Apr. 2017.

[55] M. K. Karkkainen, "Subcell FDTD modeling of electrically thin dispersive layers," *IEEE Trans. Microw. Theory Tech.*, vol. 51, no. 6, pp. 1774–1780, Jun. 2003.

[56] V. Nayyeri, M. Soleimani, and O. M. Ramahi, "Modeling graphene in the finite-difference time-domain method using a surface boundary condition," *IEEE Trans. Antennas Propag.*, vol. 61, no. 8, pp. 4176–4182, Aug. 2013.

[57] V. Nayyeri, M. Soleimani, and O. M. Ramahi, "Wideband modeling of graphene using the finite-difference time-domain method," *IEEE Trans. Antennas Propag.*, vol. 61, no. 12, pp. 6107–6114, Dec. 2013.

[58] H. Lin, M. F. Pantoja, L. D. Angulo, J. Alvarez, R. G. Martin, and S. G. Garcia, "FDTD modeling of graphene devices using complex conjugate dispersion material model," *IEEE Microw. Wireless Compon. Lett.*, vol. 22, no. 12, pp. 612–614, Dec. 2012.

[59] D.-W. Wang, W.-S. Zhao, X.-Q. Gu, W. Chen, and W.-Y. Yin, "Wideband modeling of graphene-based structures at different temperatures using hybrid FDTD method," *IEEE Trans. Nanotechnol.*, vol. 14, no. 2, pp. 250–258, Mar. 2015.

[60] Y. Guo, T. Zhang, W.-Y. Yin, and X.-H. Wang, "Improved hybrid FDTD method for studying tunable graphene frequency-selective surfaces (GFSS) for THz-wave applications," *IEEE Trans. THz Sci. Technol*, vol. 5, no. 3, pp. 358–367, May 2015.

[61] B. Salski, "An FDTD model of graphene intraband conductivity," *IEEE Trans. Microw. Theory Tech.*, vol. 62, no. 8, pp. 1570–1578, Aug. 2014.

[62] X.-H. Wang, W.-Y. Yin, and Z. Z. D. Chen, "One-step leapfrog ADI-FDTD method for simulating electromagnetic wave propagation in general dispersive media," *Opt. Express*, vol. 21, no. 18, pp. 20565–20576, Sep. 2013.

[63] I. Ahmed, E. H. Khoo, and E. Li, "Efficient modeling and simulation of graphene devices with the LOD-FDTD method," *IEEE Microw. Wireless Compon. Lett.*, vol. 23, no. 6, pp. 306–308, Jun. 2013.

[64] X.-H. Wang, W.-Y. Yin, and Z. Chen, "Matrix exponential FDTD modeling of magnetized graphene sheet," *IEEE Antennas Wireless Propag. Lett.*, vol. 12, pp. 1129–1132, 2013.

[65] K. Niu, Z. Huang, M. Li, and X. Wu, "Optimization of the artificially anisotropic parameters in WCS-FDTD method for reducing numerical dispersion," *IEEE Trans. Antennas Propag.*, vol. 65, no. 12, pp. 7389–7394, Dec. 2017.

[66] K. Niu, Z. Huang, X. Ren, M. Li, B. Wu, and X. Wu, "An optimized 3-D HIE-FDTD method with reduced numerical dispersion," *IEEE Trans. Antennas Propag.*, vol. 66, no. 11, pp. 6435–6440, Nov. 2018.

[67] K. Niu, Z. Huang, B. Wu, and X. Wu, "3D optimised hybrid implicit–explicit FDTD method with suppressed numerical dispersion," *Electron. Lett.*, vol. 54, no. 6, pp. 335–336, Mar. 2018.

[68] J. Chen, N. Xu, A. Zhang, and J. Guo, "Using dispersion HIE-FDTD method to simulate the graphene-based polarizer," *IEEE Trans. Antennas Propag.*, vol. 64, no. 7, pp. 3011–3017, Jul. 2016.

[69] J. Chen, J. Li, and Q. H. Liu, "Analyzing graphene-based absorber by using the WCS-FDTD method," *IEEE Trans. Microw. Theory Tech.*, vol. 65, no. 10, pp. 3689–3696, Oct. 2017.

[70] M.-L. Zhai, H.-L. Peng, X.-H. Wang, X. Wang, Z. Chen, and W.-Y. Yin, "The conformal HIE-FDTD method for simulating tunable graphene-based couplers for THz applications," *IEEE Trans. THz Sci. Technol*, vol. 5, no. 3, pp. 368–376, May 2015.

[71] G. D. Bouzianas, N. V. Kantartzis, C. S. Antonopoulos, and T. D. Tsiboukis, "Optimal modeling of infinite graphene sheets via a class of generalized FDTD schemes," *IEEE Trans. Magn.*, vol. 48, no. 2, pp. 379–382, Feb. 2012.

[72] X. Yu and C. D. Sarris, "A perfectly matched layer for subcell FDTD and applications to the modeling of graphene structures," *IEEE Antennas Wireless Propag. Lett.*, vol. 11, pp. 1080–1083, 2012.

[73] M. Feizi, V. Nayyeri, and O. M. Ramahi, "Modeling magnetized graphene in the finite-difference time-domain method using an anisotropic surface boundary condition," *IEEE Trans. Antennas Propag.*, vol. 66, no. 1, pp. 233–241, Jan. 2018.

[74] J.-M. Jin, *The Finite Element Method in Electromagnetics*. Hoboken, NJ, USA: Wiley, 2015.

[75] C. M. Studio, CST GmbH, Ilsenburg, Germany, 2016.

[76] C. Multiphysics, Comsol, Inc., Stockholm, Sweden 2005.

[77] H. Ansys, Ansoft Corp., Pittsburgh, PA, USA, 2015.

[78] M. Amin, M. Farhat, and H. Bagci, "An ultra-broadband multilayered graphene absorber," *Opt. Express*, vol. 21, no. 24, pp. 29938–29948, Dec. 2013.

[79] A. B. Khanikaev, R. Fleury, S. H. Mousavi, and A. Alu, "Topologically robust sound propagation in an angular-momentum-biased graphene-like resonator lattice," *Nature Commun.*, vol. 6, Oct. 2015, Art. no. 8260.

[80] R. C. Rollings, A. T. Kuan, and J. A. Golovchenko, "Ion selectivity of graphene nanopores," *Nature Commun.*, vol. 7, Apr. 2016, Art. no. 11408.

[81] J. Li *et al.*, "Gate-controlled topological conducting channels in bilayer graphene," *Nature Nanotechnol.*, vol. 11, no. 12, pp. 1060–1065, Aug. 2016.

[82] Z. Yan, G. Liu, J. M. Khan, and A. A. Balandin, "Graphene quilts for thermal management of high-power GaN transistors," *Nature Commun.*, vol. 3, May 2012, Art. no. 827.

[83] N. Liu, G. Cai, L. Ye, and Q. H. Liu, "The efficient mixed FEM with the impedance transmission boundary condition for graphene plasmonic waveguides," *J. Lightw. Technol.*, vol. 34, no. 23, pp. 5363–5370, Mar. 2016.

[84] M. Feliziani, S. Cruciani, and F. Maradei, "Circuit-oriented FEM modeling of finite extension graphene sheet by impedance network boundary conditions (INBCs)," *IEEE Trans. THz Sci. Technol*, vol. 4, no. 6, pp. 734–740, Nov. 2014.

[85] P. Li, Y. Shi, L. J. Jiang, and H. Bagci, "DGTD analysis of electromagnetic scattering from penetrable conductive objects with IBC," *IEEE Trans. Antennas Propag.*, vol. 63, no. 12, pp. 5686–5697, Dec. 2015.

[86] P. Li, L. J. Jiang, and H. Bagci, "Transient analysis of dispersive power-ground plate pairs with arbitrarily shaped antipads by the DGTD method with wave port excitation," *IEEE Trans. Electromagn. Compat.*, vol. 59, no. 1, pp. 172–183, Feb. 2016.

[87] P. Li and L. J. Jiang, "Integration of arbitrary lumped multiport circuit networks into the discontinuous Galerkin time-domain analysis," *IEEE Trans. Microw. Theory Tech.*, vol. 61, no. 7, pp. 2525–2534, Jul. 2013.

[88] K. Sankaran, "Accurate domain truncation techniques for time-domain conformal methods," Ph.D. dissertation, ETH Zurich, Zurich, Switzerland, 2007.

[89] P. Li, L. J. Jiang, Y. J. Zhang, S. Xu, and H. Bagci, "An efficient mode-based domain decomposition hybrid 2-D/Q-2D finite-element time-domain method for power/ground plate-pair analysis," *IEEE Trans. Microw. Theory Tech.*, vol. 66, no. 10, pp. 4357–4366, Oct. 2018.

[90] P. Li, L. J. Jiang, and H. Bagci, "A resistive boundary condition enhanced DGTD scheme for the transient analysis of graphene," *IEEE Trans. Antennas Propag.*, vol. 63, no. 7, pp. 3065–3076, Jul. 2015.

[91] B. Gustavsen and A. Semlyen, "Rational approximation of frequency domain responses by vector fitting," *IEEE Trans. Power Del.*, vol. 14, no. 3, pp. 1052–1061, Jul. 1999.

[92] P. Li and L. J. Jiang, "Modeling of magnetized graphene from microwave to THz range by DGTD with a scalar RBC and an ADE," *IEEE Trans. Antennas Propag.*, vol. 63, no. 10, pp. 4458–4467, Oct. 2015.

[93] P. Wang, Y. Shi, C.-Y. Tian, and L. Li, "Analysis of graphene-based devices using wave equation based discontinuous Galerkin time-domain method," *IEEE Antennas Wireless Propag. Lett.*, vol. 17, no. 12, pp. 2169–2173, Dec. 2018.

[94] R. F. Harrington, *Field Computation by Moment Methods*. Hoboken, NJ, USA: Wiley, 1993.

[95] J. Song, C.-C. Lu, and W. C. Chew, "Multilevel fast multipole algorithm for electromagnetic scattering by large complex objects," *IEEE Trans. Antennas Propag.*, vol. 45, no. 10, pp. 1488–1493, Oct. 1997.

[96] A. E. Yilmaz, J.-M. Jin, and E. Michielssen, "Time domain adaptive integral method for surface integral equations," *IEEE Trans. Antennas Propag.*, vol. 52, no. 10, pp. 2692–2708, Oct. 2004.

[97] Y. P. Chen, W. E. Sha, L. Jiang, and J. Hu, "Graphene plasmonics for tuning photon decay rate near metallic split-ring resonator in a multilayered substrate," *Opt. Express*, vol. 23, no. 3, pp. 2798–2807, Feb. 2015.

[98] O. V. Shapoval, J. S. Gomez-Diaz, J. Perruisseau-Carrier, J. R. Mosig, and A. I. Nosich, "Integral equation analysis of plane wave scattering by coplanar graphene-strip gratings in the THz range," *IEEE Trans. THz Sci. Technol*, vol. 3, no. 5, pp. 666–674, Sep. 2013.

[99] M. V. Balaban, O. V. Shapoval, and A. I. Nosich, "Thz wave scattering by a graphene strip and a disk in the free space: Integral equation analysis and surface plasmon resonances," *J. Opt.*, vol. 15, no. 11, Oct. 2013, Art. no. 114007.

[100] R. Araneo, G. Lovat, S. Celozzi, and P. Burghignoli, "Crosstalk analysis in graphene multiconductor transmission lines," in *Proc. IEEE Int. Symp. Electromagn. Compat.*, Aug. 2014, pp. 28–32.

[101] G. Lovat, R. Araneo, P. Burghignoli, and G. W. Hanson, "Fundamental properties of plasmonic propagation in graphene nanoribbons," in *Proc. IEEE 15th Int. Conf. Nanotechnol.*, Jul. 2015, pp. 176–179.

[102] Y. Shi, I. E. Uysal, P. Li, H. A. Ulku, and H. Bagci, "Analysis of electromagnetic wave interactions on graphene sheets using time domain integral equations," in *Proc. 31st Int. Rev. Prog. Appl. Computat. Electromagn.*, May 2015, pp. 1–2.
[103] Y. Zhao, S. Tao, D. Ding, and R. Chen, "A time-domain thin dielectric sheet (TD-TDS) integral equation method for scattering characteristics of tunable graphene," *IEEE Trans. Antennas Propag.*, vol. 66, no. 3, pp. 1366–1373, Dec. 2018.
[104] A. E. Ruehli, "Equivalent circuit models for three-dimensional multiconductor systems," *IEEE Trans. Microw. Theory Tech.*, vol. 22, no. 3, pp. 216–221, Mar. 1974.
[105] Y. S. Cao, L. J. Jiang, and A. E. Ruehli, "An equivalent circuit model for graphene-based terahertz antenna using the PEEC method," *IEEE Trans. Antennas Propag.*, vol. 64, no. 4, pp. 1385–1393, Apr. 2016.
[106] Y. S. Cao, P. Li, L. J. Jiang, and A. E. Ruehli, "The derived equivalent circuit model for magnetized anisotropic graphene," *IEEE Trans. Antennas Propag.*, vol. 65, no. 2, pp. 948–953, Feb. 2016.
[107] D. Romano and G. Antonini, "Partial element equivalent circuit-based transient analysis of graphene-based interconnects," *IEEE Trans. Electromagn. Compat.*, vol. 58, no. 3, pp. 801–810, Jun. 2016.
[108] F. Ling, C.-F. Wang, and J.-M. Jin, "An efficient algorithm for analyzing large-scale microstrip structures using adaptive integral method combined with discrete complex-image method," *IEEE Trans. Microw. Theory Techn.*, vol. 48, no. 5, pp. 832–839, May 2000.
[109] B. Shanker, A. A. Ergin, M. Lu, and E. Michielssen, "Fast analysis of transient electromagnetic scattering phenomena using the multilevel plane wave time domain algorithm," *IEEE Trans. Antennas Propag.*, vol. 51, no. 3, pp. 628–641, Mar. 2003.
[110] S. Sun and D. Jiao, "First-principles based multiphysics modeling and simulation of on-chip Cu-Graphene hybrid nano-interconnects in comparison with simplified model based analysis," *IEEE J. Multiscale Multiphys. Comput. Techn.*, vol. 4, pp. 374–382, 2019.
[111] S. Sun and D. Jiao, "Multiphysics modeling and simulation of 3-D Cu-Graphene hybrid nanointerconnects," *IEEE Trans. Microw. Theory Tech.*, vol. 69 no. 2, pp. 490–500, Feb. 2020.
[112] J. W. You and N. C. Panoiu, "Plasmon-induced nonlinearity enhancement and homogenization of graphene metasurfaces," *Opt. Lett.*, vol. 44, no. 12, pp. 3030–3033, Jun. 2019.
[113] L. Yang, J. Tian, K. Z. Rajab, and Y. Hao, "FDTD modeling of nonlinear phenomena in wave transmission through graphene," *IEEE Antennas Wireless Propag. Lett.*, vol. 17, no. 1, pp. 126–129, Jan. 2018.
[114] A. M. Attiya, "Modeling nonlinear electrical conductivity of graphene by using finite difference time domain," in *Proc. 33rd Nat. Radio Sci. Conf.*, 2016, pp. 340–347.
[115] S. A. Mikhailov and K. Ziegler, "Nonlinear electromagnetic response of graphene: Frequency multiplication and the self-consistent-field effects," *J. Phys.: Condens. Matter*, vol. 20, no. 38, Aug. 2008, Art. no. 384204.
[116] S. A. Mikhailov, "Non-linear electromagnetic response of graphene," *Europhys. Lett*, vol. 79, no. 2, Jun. 2007, Art. no. 27002.

Kaikun Niu (Member, IEEE) was born in Huainan, China, in 1992. He received the B.S. and Ph.D. degree in electronic engineering from Anhui University (AHU), Hefei, China, in 2014 and 2019, respectively.

In 2017, he was a Research Assistant with the Department of Electrical and Electronic Engineering, The University of Hong Kong (HKU), Hong Kong. From 2018 to 2019, he was a Visiting Student with King Abdullah University of Science and Technology, Thuwal, Saudi Arabia, where he is currently a Postdoctoral Research Fellow. His current research interests include computational electromagnetics, electromagnetic compatibility, metamaterials, and nonlinear plasmonic.

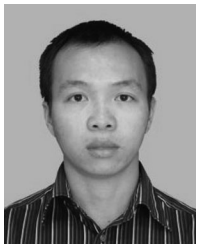

Ping Li (Senior Member, IEEE) received the Ph.D. degree from the University of Hong Kong (HKU), Hong Kong, in 2014.

Since 2014, he was a Postdoctoral Fellow with King Abdullah University of Science and Technology (KAUST), Thuwal, Saudi Arabia, and Purdue University, West Lafayette, IN, USA. From 2017 to 2018, he was a Research Assistant Professor with HKU. He is currently an Associate Professor with the Shanghai Jiao Tong University (SJTU). He has also been an Honorary Assistant Professor with HKU since 2017. His current research interests include computational electromagnetics, electromagnetic compatibility, and signal/power integrity.

Dr. Li was the recipient of various awards, including the Student Paper Award in 2014 Int. FEM Workshop, 2018 Best Paper Prize of the Chinese Journal of Radio Science, and Young Scientist Award in the 2018 Joint IEEE EMC&APEMC, 2018 ACES-China, and 40th PIERS, respectively. His research project also received the Second Prize of Natural Science given by the Chinese Institute of Electronics in 2019.

Zhixiang Huang (Senior Member, IEEE) was born in Anhui, China, in 1979. He received the B.S. and Ph.D. degrees from Anhui University (AHU), Hefei, China, in 2002 and 2007, respectively.

Since 2008, he has been a Full Professor with the School of Electronic Information and Engineering, AHU. From September 2010 to September 2011, he was a Visiting Scholar with Iowa State University, Ames, IA, USA. From August 2013 to October 2013, he was a Visiting Professor with the University of Hong Kong. From February 2014 to February 2015, he was a Visiting Professor with the Beijing National Laboratory for Condensed Matter Physics, Institute of Physics, Chinese Academy of Sciences. He has coauthored one monograph on the symplectic finite-difference time-domain method and two book chapters for CRC Press and InTech Publishers. He has coauthored 70 peer-reviewed journal papers included in the Web of Science Core Collection. His current research interests include time-domain numerical methods, metamaterials, and active metamaterials.

Dr. Huang was the recipient of the Second Prize of Science and Technology from the Anhui Province Government, China, in 2015. He was also the recipient of the National Science Foundation for Outstanding Young Scholar of China in 2017.

Li Jun Jiang (Fellow, IEEE) received the B.S. degree in electrical engineering from the Beijing University of Aeronautics and Astronautics, Beijing, China, in 1993, the M.S. degree from the Tsinghua University, Beijing, in 1996, and the Ph.D. degree from the University of Illinois at Urbana-Champaign, Champaign, IL, USA, in 2004.

From 1996 to 1999, he was an Application Engineer with the Hewlett-Packard Company, Palo Alto, CA, USA. Since 2004, he has been the Postdoctoral Researcher, the research staff member, and the Senior Engineer with IBM T.J. Watson Research Center. Since the end of 2009, he has also been an Associate Professor with the Department of Electrical and Electronic Engineering, the University of Hong Kong, Hong Kong.

Dr. Jiang was the recipient of the IEEE MTT Graduate Fellowship Award in 2003 and Y.T. Lo Outstanding Research Award in 2004. He is an Associate Editor for the IEEE TRANSACTIONS ON ANTENNAS AND PROPAGATION, the Associate Editor for *Progress in Electromagnetics Research*, the Associate Guest Editor for the Proceedings of IEEE Special Issue in 2011–2012, an IEEE AP-S Member, an IEEE MTT-S member, an IEEE EMC-S member, an ACES member, and a member of Chinese Computational Electromagnetics Society. He was the Semiconductor Research Cooperation (SRC) Industrial Liaison for several academic projects. He served as the Scientific Consultant to Hong Kong ASTRI (Hong Kong Applied Science and Technology Research Institute Company Limited) in 2010–2011, the Panelist of the Expert Review Panel (ERP) of Hong Kong R and D Centre for Logistics and Supply Chain Management Enabling Technologies since January 1, 2013. He is also the Senior Visiting Professor at Tsinghua University since Jun. 2013. He was the TPC Chair of the 7th International Conference on Nanophotonics (ICNP)/the 3rd Conference on Advances in Optoelectronics and Micro/Nano Optics (AOM), the TPC Co-Chair of the 12th International Workshop on Finite Elements for Microwave Engineering, the Co-Chair of 2013 International Workshop on Pulsed Electromagnetic Field at Delft, the Netherlands, the General Chair of 2014 IEEE 14th HK AP/MTT Postgraduate Conference. He was the elected TPC member of IEEE EPEP since 2014, the TPC member of IEEE EDAPS since 2010, the TPC member of 2013 IEEE ICMTCE, the scientific committee member of 2010 IEEE SMEE, the Special Session Organizer of IEEE EDAPS, IEEE EMC, ACES, AP-RASC, PIERS, Co-Organizer of HKU Computational Science and Engineering Workshops in 2010–2012, the TC-9 and TC-10 member of IEEE EMC-S since 2011, and Session Chairs of many international conferences. He also serves as the Reviewer of IEEE Transactions on several topics, and other primary electromagnetics and microwave related journals. He has been working collaboratively with many international researchers.

Hakan Bagci (Senior Member, IEEE) received the B.S. degree in electrical and electronics engineering from the Bilkent University, Ankara, Turkey, in 2001, and the M.S. and Ph.D. degrees from the University of Illinois at Urbana-Champaign (UIUC), Urbana, IL, USA, in 2003 and 2007, respectively, both in electrical and computer engineering.

From June 1999 to July 2001, he was an Undergraduate Researcher with the Computational Electromagnetics Group, Bilkent University. From August 2001 to December 2006, he was a Research Assistant with the Center for Computational Electromagnetics and Electromagnetics Laboratory, UIUC. From January 2007 to August 2009, he was a Research Fellow with the Radiation Laboratory, University of Michigan, Ann Arbor, MI, USA. Since August 2009, he has been with the King Abdullah University of Science and Technology (KAUST), Thuwal, Saudi Arabia, where he is currently an Associate Professor of Electrical Engineering. His research interests include various aspects of theoretical and applied computational electromagnetics with emphasis on well-conditioned frequency and time domain integral equation formulations and their discretization, hybrid time domain integral and differential equation solvers, accurate, stable, and efficient marching schemes for time domain solvers, stochastic characterization of electromagnetic field and wave interactions on complex geometries, and solution of 2- and 3-dimensional electromagnetic inverse scattering problem using signal processing techniques. He authored or coauthored more than 90 journal papers and more than 200 papers in conference proceedings.

Dr. Bagci was the recipient of the 2008 International Union of Radio Scientists (URSI) Young Scientist Award and 2004–2005 Interdisciplinary Graduate Fellowship from the Computational Science and Engineering Department, UIUC. His paper titled "Fast and Rigorous Analysis of EMC/EMI Phenomena on Electrically Large and Complex Structures Loaded With Coaxial Cables" was one of the three finalists (with honorable mention) for the 2008 Richard B. Schulz Best Transactions Paper Award given by the IEEE Electromagnetic Compatibility Society. He authored (as student) or coauthored (as student and advisor) 17 finalist/honorable mention papers in the student paper competitions at the 2005, 2008, 2010, 2014, 2015, 2016, 2017, 2018 IEEE Antennas and Propagation Society International Symposiums and 2013, 2014, 2016, 2017, and 2018 Applied Computational Electromagnetics Society Conferences. He is currently an Associate Editor for the IEEE TRANSACTIONS ON ANTENNAS AND PROPAGATION, IEEE JOURNAL ON MULTISCALE AND MULTIPHYSICS COMPUTATIONAL TECHNIQUES, and IEEE ANTENNAS AND PROPAGATION MAGAZINE.